Weierstraß-Institut

für Angewandte Analysis und Stochastik

Leibniz-Institut im Forschungsverbund Berlin e. V.

Preprint ISSN 0946 – 8633

Filamentary pulse self-compression: The impact of the cell windows

Carsten Brée[1,2], Ayhan Demircan[1], Jens Bethge[2], Erik T. J. Nibbering[2],

Stefan Skupin[3,4], Luc Bergé[5], Günter Steinmeyer[2,6]

submitted: April 27, 2011

[1] Weierstrass Institute, Mohrenstraße 39, 10117 Berlin, Germany
E-Mail: carsten.bree@wias-berlin.de
ayhan.demircan@gmx.de (A. Demircan was a collaborator at WIAS until Dec. 2010)

[2] Max Born Institute for Nonlinear Optics and Short Pulse Spectroscopy, 12489 Berlin, Germany
E-Mail: bethge@mbi-berlin.de
nibbering@mbi-berlin.de
steinmey@mbi-berlin.de

[3] Max-Planck-Institut für Physik komplexer Systeme, 01187 Dresden, Germany
E-Mail: skupin@mpipks-dresden.mpg.de

[4] Institut für Festkörpertheorie und -optik, Friedrich-Schiller-Universität, 07743 Jena, Germany

[5] CEA-DAM, DIF, 91297 Arpajon, France
E-Mail: luc.berge@cea.fr

[6] Optoelectronics Research Centre, Tampere University of Technology, 33101 Tampere, Finland

No. 1606

Berlin 2011

2010 *Mathematics Subject Classification.* Primary 78A60.

2010 *Physics and Astronomy Classification Scheme.* 42.65.-k,42.65.Jx,42.65.Re.

Key words and phrases. Nonlinear Optics, Femtosecond Filamentation, Pulse compression.

Financial support by the Deutsche Forschungsgemeinschaft, grants DE 1209/1-2 and STE 762/7-2, is gratefully acknowledged. GS gratefully acknowledges support by the Academy of Finland (project grant 128844).

Edited by
Weierstraß-Institut für Angewandte Analysis und Stochastik (WIAS)
Leibniz-Institut im Forschungsverbund Berlin e. V.
Mohrenstraße 39
10117 Berlin
Germany

Fax: +49 30 2044975
E-Mail: preprint@wias-berlin.de
World Wide Web: http://www.wias-berlin.de/

Abstract

Self-compression of multi-millijoule laser pulses during filamentary propagation is usually explained by the interplay of self-focusing and defocusing effects, causing a substantial concentration of energy on the axis of the propagating optical pulse. Recently, it has been argued that cell windows may play a decisive role in the self-compression mechanism. As such windows have to be used for media other than air their presence is often unavoidable, yet they present a sudden non-adiabatic change in dispersion and nonlinearity that should lead to a destruction of the temporal and spatial integrity of the light bullets generated in the self-compression mechanism. We now experimentally prove that there is in fact a self-healing mechanism that helps to overcome the potentially destructive consequences of the cell windows. We show in two carefully conducted experiments that the cell window position decisively influences activation or inhibition of the self-healing mechanism. A comparison with a windowless cell shows that presence of this mechanism is an important prerequisite for the exploitation of self-compression effects in windowed cells filled with inert gases.

1 Introduction

Increasing the energy concentration in a short light pulse has been an active area of research for nearly 30 years. Active pulse compression [1] is a key method that combines spectral broadening due to the nonlinear optical effect of self-phase modulation with subsequent linear dispersion compensation to produce a shorter pulse. Originally, this method employs optical fibers, limiting input pulse energies to a few microjoules. Using hollow fibers filled with noble gases [2, 3] allowed scaling pulse compression to about one millijoule at kHz pulse repetition rates, with pulse durations reaching values below 4 fs [4]. Using a pressure gradient at 20 Hz repetition rate, sub-10 fs pulse durations with up to 5 mJ pulse energy could be demonstrated [5]. Nevertheless, while the hollow fiber increases the effective nonlinear interaction length, damage of this structure also implies a severe limitation of pulse compression methods in terms of pulse energy. This has brought up several approaches [6, 7] to use the nonlinearity of noble gases in non-guided geometries together with suitable dispersion compensation for the compression of short and energetic pulses. While all these schemes rely on separate nonlinear spectral broadening and dispersion compensation, self compression of ultrashort laser pulses during filamentary propagation is an interesting alternative for the generation of sub-10 fs pulses with energies up to a few millilioules [8, 9, 10, 11]. As the filament is a self-generated waveguide structure, it cannot be damaged, which allows for the compression of significantly higher energise than can be transmitted through hollow waveguides. Moreover, unlike hollow waveguide compression schemes that rely on nonlinear spectral broadening and subsequent dispersion compensation, the self-compression technique does not require any means of dispersion control like chirped mirrors or grating compressors [12].

Even though self-compression is now well understood through numerical simulations, there are several aspects that could not be satisfactorily explained so far. One of these aspects is the role of the windows of noble-gas filled filament cells, in particular their output window. As nonlinearity and dispersion in the window are about three orders of magnitude higher than in the gas cell, the

pulses experience a sudden nonadiabatic change of linear and nonlinear optical properties. One would expect that such a massive change would immediately destroy the temporal signature of the short pulse and may even cause a break-up of the spatial profile. A recent theoretical analysis [13, 14] revealed, however, that a self-healing process restores the favorable properties of the short pulses in the subsequent propagation in atmospheric air or even vacuum. Any experimental proof for a strong effect of the windows is still outstanding. In the following, we present two test experiments to verify the importance of the output window. Even though it is impossible to monitor the self-healing process directly after transmission through the window, we find supporting evidence for this process in more indirect measurements.

2 Experimental procedure

Our experimental setup consisted of a Ti:sapphire regenerative amplifier delivering 45 fs pulses with 5 mJ pulse energy, with a collimated beam waist $w_0 = 9$ mm. Focusing the pulsed laser beam with an $R = 3$ m concave mirror into an argon-filled, 1.5 m long gas cell at atmospheric pressure, an approximately 40 cm long filament is formed, with a reddish violet fluorescent trail starting at about 10 cm before the geometrical focus. Appearance of the characteristic fluorescence also seen in an argon discharge is taken as an indication for intensities that are high enough to cause ionization of argon. In order to achieve a single stable filament, a central part of the input beam is selected by an adjustable aperture. The optical power transmitted through this first aperture was measured as 1.4 W, which at a repetition rate of 1 kHz corresponds to a pulse energy of 1.4 mJ and to a peak pulse power of 30 GW. This equals three critical powers for self-focusing in argon at 800 nm. At the output of the gas-cell, a pulse energy of 1.2 mJ was measured. The beam enters and leaves the gas cell by traversing 500 μm thick Brewster-angled silica windows, which were later replaced by 50 μm thick polypropylene foils. As filamentary self-compression dynamics is most pronounced in the spatial center of the beam, we carefully matched a second aperture to select the white-light core of the beam, which contains a pulse energy of 0.6 mJ. For diagnosis of the filament cell output, we used a simple spectrograph and spectral phase interferometry for direct electric-field reconstruction (SPIDER, [15, 16, 17, 18]). In order to avoid damage in the nonlinear crystal of the SPIDER setup, we attenuated the beam using the front reflex off a silica wedge. As the subsequent experiments strongly rely on the accuracy of the SPIDER data, we carefully analyzed the statistical fluctuations of the reconstructed pulse shapes using the output pulses from the self-generated filament in a first step. Figure 1(a) shows a recorded interferogram (solid line) and the standard deviation (dashed line) of the reconstructed group delay, calculated from a set of approximately 50 measured interferograms. Here the SPIDER trace is detected at the second harmonic of the input wavelength, i.e., at about 750 THz, since the SPIDER method relies on the generation of two spectrally sheared, upconverted copies of the pulse by sum frequency generation in a $\chi^{(2)}$-medium. The corresponding spectrum and integrated spectral phase, averaged over the available data, are shown in Fig. 1(b). In the time domain, Fig. 1(c) shows the temporal intensity profile (strong solid line) reconstructed from the averaged phase. The measured pulses clearly exhibit the well-known characteristic asymmetry of filamentary light bullets [19, 20], with a duration (FWHM) of 19 fs. In addition, we display the pulse profiles corresponding to the set of measured interferograms (light gray lines) in the same figure. These measurements show that the modulation depth of the measured SPIDER traces is high enough to yield sufficient accuracy over the relevant spectral range, in particular in the extended blue wing of the spectrum. For the pulse shown, this gives rise to an error in pulse duration not exceeding ± 1 fs.

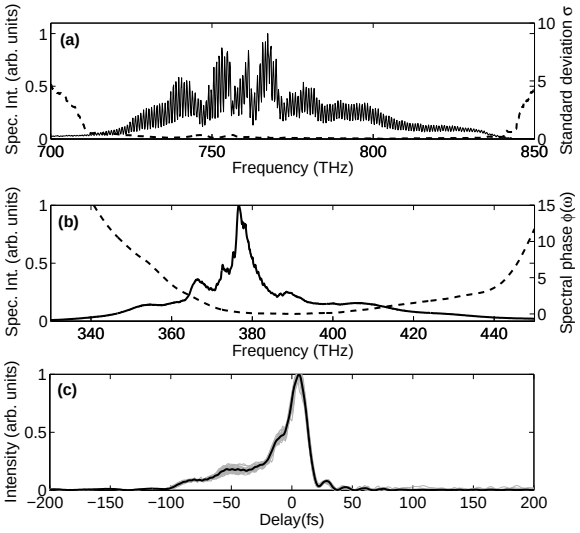

Figure 1: (a) Measured SPIDER interferogram versus frequency $\nu = \omega/2\pi$ (solid line) and standard deviation of spectral phases (dashed line) retrieved from a set of ≈ 50 interferograms. (b) Spectrum of a self-compressed pulse emerging from a filament (solid line). Dashed line shows the averaged spectral phase. Concave phases indicate excess normal dispersion. (c) Time domain representation of the measured pulse. The black line shows the reconstruction using the averaged spectral phase. The light gray lines show pulse profiles reconstructed from each measured interferogram.

3 Experiment 1: variation of window position

In a first experiment we vary the position of the entire argon cell along the optical axis. In particular, this measure varies the distance between the plasma column and the output window, but leaves the linear dispersion of the system unaffected. The window position Δz is defined as the distance between the inner surface of the silica output window of the cell and the position of the geometrical focus. The quantity Δz is varied between $\Delta z = 103$ and 111 cm, the maximum variation allowed due to practical constraints in our setup. The results of the measurements are summarized in Fig. 2. In Fig. 2(a), the measured spectra at minimum and maximum Δz are shown. This comparison clearly reveals that a decrease of Δz comes along with an elevated red shoulder of the spectrum, while the blue shoulder generated by self-phase modulation and self-steepening in the trailing part of the pulse appears suppressed. In fact, an analogous behavior was observed in the numerical simulations of Ref. [14]. We can also see significant changes in the SPIDER measurements. As SPIDER is insensitive for variations of the offset and linear slope of the spectral phase $\Phi(\omega)$, we discuss its second derivative, i.e., the group delay dispersion (GDD)defined as $D_2(\omega) = \partial^2\Phi(\omega)/\partial\omega^2$. Figure 2(b) displays the dependence of the measured GDD on the window position Δz in a frequency range from 340 to 420 THz. This comparison shows that the GDD exhibits strong fluctuations, especially in the red spectral range, i.e., below a carrier frequency of 375 THz. In fact, the smaller absolute values and the weak variation of the GDD on the blue side of the spectrum is well expected from the asymmetric spectral broadening due to self-steepening experienced by pulses in the few-cycle domain, as the new blue spectral content is generated in the self-steepened trailing part of the pulse and is thus strongly localized in the time domain. In the frequency domain, this strong localization is evidenced by a nearly flat spectral phase in the blue part of the spectrograms, a feature which has been verified experimentally several times [19, 8, 9]. Reconstructing temporal pulse profiles from measured spectra and phases, as shown in Fig. 2(c), the pulse duration is

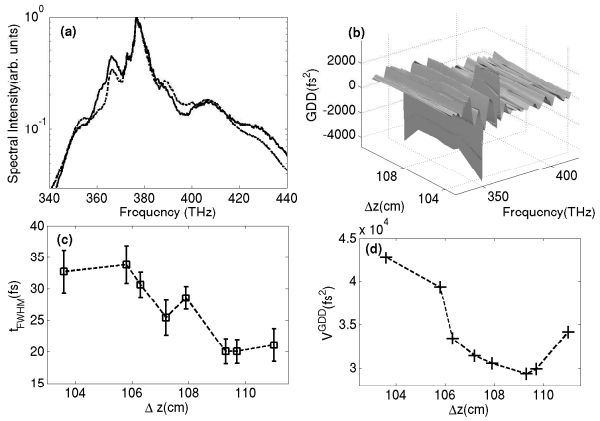

Figure 2: (a) Comparison of measured spectra for small (solid line) and large (dashed line) values of Δz. Window proximity elevates the red spectral wing on the expense of the blue wing. (b) Variation of GDD versus the window position Δz. (c) Measured pulse duration versus Δz. (d) Total variation V^{GDD} calculated according to Eq. (1) in the frequency range from 340 to 425 THz.

constant within experimental precision for large window-filament distance $\Delta z > 109\,$cm. However, a reduction of Δz results in an increasing pulse duration. At $\Delta z \leq 106\,$cm, we observe only poor compression ratios, with pulse durations exceeding $30\,$fs. In the following, we use the functional

$$V^{\mathrm{GDD}}(\omega_1, \omega_2) = \int_{\omega_1}^{\omega_2} \left| \frac{dD_2(\omega)}{d\omega} \right| d\omega \tag{1}$$

as a quantitative measure of the total variation, where $\omega_1 = 2\pi \times 340\,$THz and $\omega_2 = 2\pi \times 425\,$THz. In Fig. 2(d), $V^{\mathrm{GDD}}(\omega_1, \omega_2)$ is plotted against Δz. From $\Delta z = 103$ to $109\,$cm, the variation roughly correlates with the pulse duration, with the exception of $\Delta z > 109\,$cm, where it increases while the pulse duration remains nearly constant. These measurements clearly show that the compression ratio strongly depends on the position of the exit window. In fact, an unsuitable choice of the window position can render filamentary self-compression unobservable. However, in order to provide evidence for the self-restoration mechanism of [13, 14], it is clearly necessary to supplement the previous measurements with experimental data of the self-compression efficiency **inside** the argon cell, which is, of course, impossible to achieve due the high intensity in the filament. Instead, output pulses from a windowless argon cell, as described in the next section, provide indirect evidence of the self-compression efficiency within the argon cell, and corroborate further the non-negligible influence of the cell windows.

4 Experiment 2: windowless measurement

In the following, the impact of the exit window is analyzed in more detail, especially the theoretically predicted dramatic temporal stretching of the pulse due to the interplay of Kerr self-focusing and GDD. To this purpose, the gas cell is positioned at $z = 103.6\,$cm, which renders self-compression ineffective (see previous Section). In a first experiment, the evacuated gas cell is carefully filled with argon until atmospheric pressure is reached. The laser beam is then coupled into the gas cell. The energy of the pulses entering the cell via the first aperture is $1.2\,$mJ. The temporal pulse profiles and spectral phases are reconstructed using the SPIDER method. In a next step, the exit window is removed from the gas cell and replaced by a $50\,\mu$m

polypropylene foil. The latter is then covered by a metal plate wetted by ethanol in order to prevent an implosion of the foil during the subsequent evacuation stage. Having evacuated the gas cell, it is carefully refilled with argon until atmospheric pressure is reached, allowing to remove the metal plate. The laser beam is then coupled into the gas cell again, with identical coupling conditions as for the windowed measurements, i.e., equal pulse energy and aperture diameter. Even though the foils are a factor 10 thinner than the previously used silica windows, we expect that nonlinearity and dispersion are nearly unchanged compared to the silica window [21]. Consequently, we do not observe a significant change in the pulse shaping dynamics. However, the thin foil can be easily perforated at slightly higher intensities, which enables experiments in a windowless cell. As the diameter of the aperture is very small and there is no pressure difference, it takes more than ten minutes before diffusion has significantly contaminated the argon inside the cell, as can be seen both, from a change of the fluorescence color as well as from a change in the supercontinuum spectrum. The following measurements have always been taken in the first few minutes of operation of the windowless cell, therefore minimizing the influence of air contamination. Moreover, as the ablation process perforating the foil has terminated and the power was subsequently reduced to restore input beam parameters of the windowed measurements, only plasma formation in the gases could play a role. The input beam parameters were carefully adjusted as to avoid the generation of a significant plasma density at the exit of the gas cell.

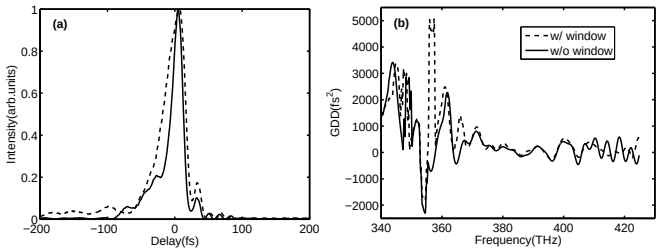

Figure 3: (a) Temporal pulse profiles and (b) GDD reconstructed from SPIDER measurements for the windowed (dashed line) and windowless case (solid line).

The results for the windowed (dashed line) and windowless cases (solid line) are directly compared in Fig. 3. In Fig. 3(a), temporal profiles are shown. In fact, the unwindowed pulse has experienced noticable self-compression, with a FWHM duration of 20 fs, while the windowed pulse is considerably longer (38 fs), confirming that for the chosen window position, self-compression is ineffective. The measurements impressively confirm the dramatic temporal stretching of the pulse due to the interplay of Kerr self-focusing and GDD, even exceeding the stretching predicted by linear theory for 0.5 mm of propagation in silica. The measured GDD for both cases is shown in Fig. 3(b). Again, the fluctuations on the red side exceed those on the blue side in both cases, yet with a stronger fluctuation for the windowed pulse. This may be attributed to self-phase modulation experienced by the pulse during silica propagation.

5 Comparison with numerical simulations

In the following, we use direct numerical simulations of the evolution equation describing filamentary propagation in order to link our experimental results to the self-restoration results of Refs. [13, 14]. For the simulations, we use the nonlinear envelope equation (NEE) [22, 9, 14] modeling the propagation of intense few-cycle pulses in noble gases, with medium parameters for argon given by Refs. [23, 24]. For a proper modeling of the experimental situation, special

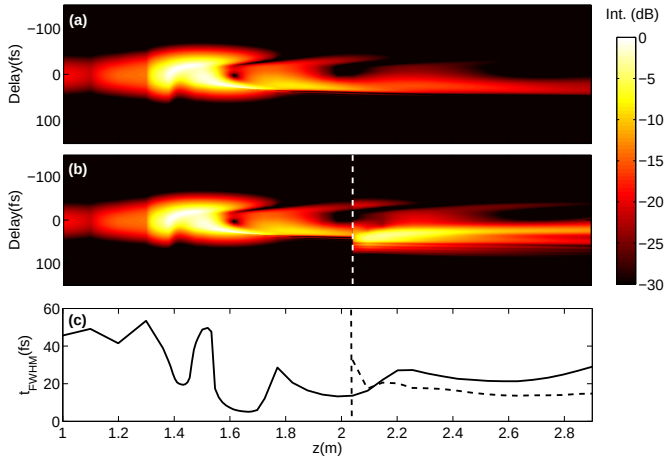

Figure 4: (Color online) (a) Evolution of the on-axis intensity profile for a fs-pulse propagating in argon. (b) Same, but with a silica window located at $z = 2.04$ m ($\Delta z = 54$ cm) and subsequent propagation in air. In (a) and (b), $0\,\mathrm{dB} \mathrel{\widehat{=}} 92\mathrm{TW/cm}^2$. (c) Evolution of pulse duration along z in argon (solid line). Dashed line: pulse duration along z for propagation in air, after traversing a 0.5 mm silica window.

care was taken with the initial conditions for the electric field distribution. In particular, as has been pointed out previously in literature [8, 25], placing an aperture in front of the entrance window stabilizes the filament, prevents spatial break-up and may help in obtaining an increased bandwidth. Additionally, Ref. [14] has pointed out the importance of including a frequency dependence of the lens factor describing the wavefront curvature of the input pulse. Considering these two issues, an appropriate choice for the Gaussian input field at $z = 0$ is given by

$$\mathcal{E}(r,t) = \sqrt{\frac{2P_{\mathrm{in}}}{\pi w_0^2}}\exp\left(-2\frac{r^2}{w_0^2} - 2\frac{r^{16}}{d_{\mathrm{ap}}^{16}}\right) \times \int_{-\infty}^{\infty} d\omega \exp\left(i\frac{\omega r^2}{2cf} + i\omega t\right)\widehat{\mathcal{E}_{\mathrm{in}}}(\omega), \tag{2}$$

where $\widehat{\mathcal{E}_{\mathrm{in}}}(\omega)$ is the Fourier transform of the assumed on-axis temporal power profile of the input pulse, $\mathcal{E}_{\mathrm{in}}(t) = \exp\left(-t^2/t_p^2\right)$. To obtain qualitative agreement with experimental data, $t_p = 38.22$ fs, $w_0 = 0.9$ mm and $d_{ap} = 0.7$ mm corresponding to the diameter of the aperture are chosen as initial conditions. The focal length is given by $f = 1.5$ m, and the input peak power P_{in} is 10.2 GW, corresponding to 8.2 critical powers and a pulse energy of 1 mJ transmitted through the aperture. The theoretical on-axis temporal profile of the initial electric field envelope, normalized to unity, is given by the Fourier transform of the spectral function $\widehat{\mathcal{E}_{\mathrm{in}}}(\omega)$. The frequency dependent lens factor in Eq. (2) accounts for the fact that different frequency components diffract into different cone angles. Initially, a simulation is performed where it is assumed that the entire propagation takes place in argon. Figure 4(a) shows the numerically simulated on-axis temporal profile along propagation distance z. Here, the well-known split-isolation scheme [26, 27] is recovered, with a temporal break-up occurring around the focal range at $z = 1.5$ m and a subsequent isolation of the trailing pulse. The solid black line in Fig. 4(c) depicts the corresponding pulse duration along z. In this simulation, self-compressed pulses are obtained with a minimum duration of ≈ 20 fs, comparable to the experimentally observed scenario. Next, the latter results are compared to those obtained by accounting for the different propagation stages, i. e. , argon, silica and air, as encountered under realistic experimental conditions. In air and silica, besides the instantaneous Kerr response $\sim n_2 I$, a delayed

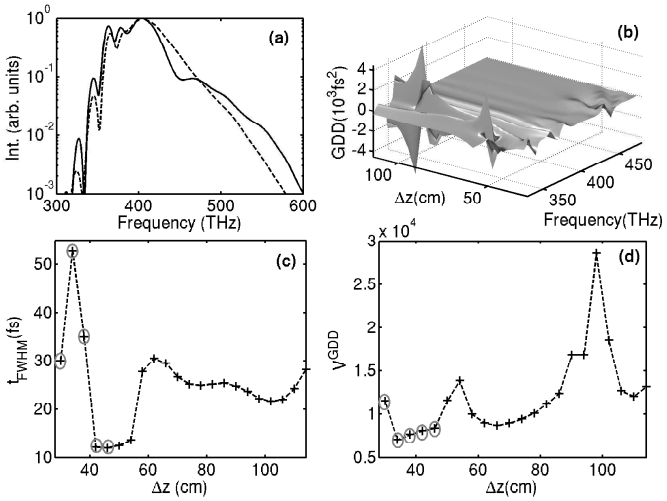

Figure 5: (Color online) (a) Comparison of simulated spectra for small ($\Delta z = 62$ cm, solid line) and large ($\Delta z = 78$ cm, dashed line) window-filament distance. Window proximity elevates the red spectral wing on the expense of the blue wing. (b) Variation of GDD versus window position Δz. (c) Simulated pulse duration versus Δz. (d) Total variation V^{GDD} calculated according to Eq. (1) in the frequency range from 340 to 425 THz. Gray circles in (c) and (d) indicate that in the corresponding configuration, the pulse fluence at the inner window surface exceeds 0.1J/cm^2, leading to significant nonlinear Fresnel reflection at the argon-silica boundary.

Raman term [28] contributes to the nonlinear polarization. The NEE is modified accordingly, with a relative contribution g of the delayed response to the total nonlinear polarization given by $g = 0.15$ in silica and $g = 0.5$ in air [29]. The latter values and all other medium parameters employed are tabulated in [14]. For the initial propagation stage in argon, $g = 0$, as no delayed Raman response is present in atomic gases. The complex output envelope of this simulation is then used as initial condition for the 0.5 mm propagation in silica. Finally, the output complex envelope is used as initial envelope for the last propagation stage in air.

As an example, Fig. 4(b) shows the evolution of the on-axis temporal intensity profile along z for this propagation sequence. Here the dashed white line marks the position of the exit window at $z = 2.04$ m, corresponding to $\Delta z = z - f = 54$ cm. This simulation reproduces simulation results of [13, 14], exhibiting temporal self-restoration. This is also evidenced by the dashed line in Fig. 4(c), exhibiting both, temporal stretching in the silica window to ≈ 33 fs from initially 14 fs, and a subsequent self-restoration of the temporal profile to 14 fs during a focusing stage. In fact, Fig. 4 indicates that the output window can even be beneficial for the pulse compression: For an optimum window position ($\Delta z = 54$ cm) the pulse duration for $z > 2.2$ m is even shorter than for the windowless case [see solid line in Fig. 4(c)]. The window position is then further varied between $\Delta z = 34$ to 110 cm, where Δz has been chosen as the distance between the inner surface of the silica window and the focal point at $f = 1.5$ m, in analogy to the experiments. The output pulses are analyzed at $z = 2.78$ m, corresponding to the fixed position of the SPIDER setup in the experiment. Figure 5(a) shows numerical spectra for $\Delta z = 62$ cm (solid line) and $\Delta z = 78$ cm (dashed line), reproducing the experimentally observed elevation of the red spectral wing and breakdown of blue spectral wing. Figure 5(b) shows the GDD along Δz. This figure qualitatively reproduces the experimental results, showing strong GDD fluctuations in the red spectral range. In contrast, the GDD on the blue side of the spectrum has a much smaller absolute value and remains nearly constant for increasing Δz, as also evidenced experimentally. The simulated pulse duration in Fig. 5(c) strongly varies with Δz, first decreasing from 50 fs to 12 fs and then increasing again up to a value of ≈ 30 fs at $\Delta z = 62$ cm.

Increasing Δz, the pulse duration decreases again to attain a minimum value of 22 fs at around $\Delta z = 100$ cm. For larger distances, the pulse duration increases again. Thus, the simulations reveal that the effectivness of filamentary self-compression crucially depends upon the chosen window position. Obviously, quantitative values for the measured and simulated pulse durations at comparable values for Δz (103–111 cm) disagree, in particular, the simulated pulse duration is almost constant in this Δz range. We attribute this discrepancy to our insufficient knowledge of the initial pulse. It is well known that pulse self-compression dynamics are very sensitive ($\sim$ 10 %) to input fluctuations [9]. However, as the experimentally measured pulse durations vary between 20 and 35 fs and decrease with increasing Δz [Fig. 2(c)], we compare them instead to simulated pulses in the range 60 cm $< \Delta z <$ 100 cm exhibiting similar durations and sign of slope with respect to the window position. This latter choice is also substantiated by the behavior of $V^{\mathrm{GDD}}(\omega_1, \omega_2)$ shown in Fig. 5(d) which, at least in the interval 60 cm $< \Delta z <$ 80 cm, roughly correlates with the pulse duration. This closely reproduces the experimentally observed behavior.

Note that in Figs. 5(c,d), for $\Delta z < 48$ cm, the pulse fluence at the inner surface of the exit window exceed 0.1 J/cm^2. According to [30, 14], this leads to significant nonlinear Fresnel reflection at the boundary, which cannot be captured by the envelope model [22, 9] employed here. Therefore, in Figs. 5(c,d), the affected data points are highlighted by gray circles, indicating that the assumed model is strictly valid only for $\Delta z > 48$ cm. An even deeper insight into

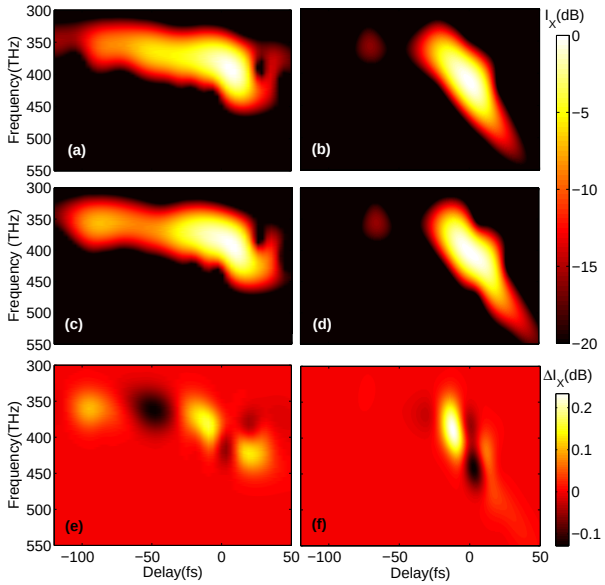

Figure 6: (Color online) XFROG spectrogram calculated from (a) measured spectrum and spectral phase at $\Delta z = 109.7$ cm and (b) corresponding figure obtained from simulation data at $\Delta z = 78$ cm. (c) Spectrogram at $\Delta z = 103.6$ cm, experiment, and (d) $\Delta z = 62$ cm, theory. (e) depicts numerical difference of experimental XFROG signals I_X, $\Delta I_X = I_X(\Delta z = 103.6\mathrm{cm}) - I_X(\Delta z = 109.7\mathrm{cm})$ shown in (a) and (c), while (f) shows the corresponding quantity for the XFROG signals shown in (b) and (d). All XFROG spectrograms normalized to unity, $0\,\mathrm{dB} \mathrel{\widehat{=}} 1$ arb. unit

the dynamics of temporal self-restoration is obtained by considering XFROG (cross-correlation frequency-resolved optical gating) spectrograms [31] both from measured and simulated pulses. Figure 6(a) shows an XFROG trace calculated from a measured spectrum and SPIDER phase, corresponding to the pulse leaving the gas cell at the exit window at $\Delta z = 109.7$ cm, a regime where self-compressed pulses with a pulse duration of 20 fs are obtained. Note that the spec-

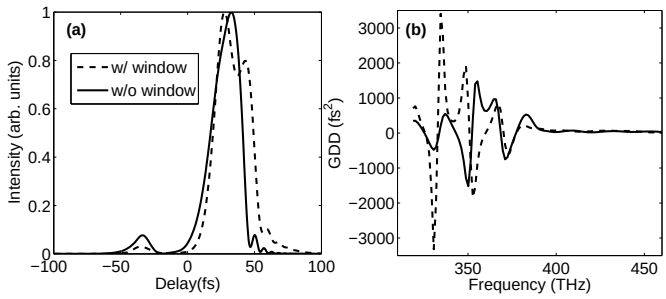

Figure 7: Simulated GDD for windowed (dashed line) and unwindowed case (solid line).

trogram exhibits the well-known inverse Γ-shape discussed in previous publications [9, 27]. In contrast, positioning the exit window at $\Delta z = 103.6\,$cm, the XFROG spectrogram reconstructed from the measured pulse is shown in Fig. 6(c). Here the refocusing of a self-compressed few-cycle pulse manifests itself in an increasing temporal delay of the blue spectral components, which eventually form a blue trailing subpulse. Indeed, this shift of the blue spectral components towards positive delay is observed in the experimental XFROG trace. As the effect is quite subtle, we plotted the numerical difference $I_X(\Delta z = 103.6\mathrm{cm}) - I_X(\Delta z = 109.7\mathrm{cm})$ between the individual XFROG intensities I_X in Fig. 6(e), which clearly confirms the previous statement. A similar result is obtained from numerical simulations by comparing numerical XFROG traces at $\Delta z = 78\,$cm [Fig. 6(b)] and $\Delta z = 62\,$cm [Fig. 6(d)]. Indeed, as revealed by the difference plot in Fig. 6(f), the blue spectral components are shifted towards positive delays. Analyzing numerical data, it turns out that the pulse at $\Delta z = 62\,$cm undergoes a stronger refocusing event after it leaves the exit window. Therefore, in fact, according to the results of [27], its blue spectral components are expected to exhibit additional positive delay. This is evidenced both in the numerical simulations and in the experiment.

To conclude, a last numerical experiment is performed where the output pulses from windowed and unwindowed configurations are compared. For the windowless case, the simulations predict a pulse duration of $\Delta t_{\mathrm{FWHM}} = 24\,$fs at $z = 2.78\,$m, whereas $\Delta t_{\mathrm{FWHM}} = 32\,$fs when a silica window is placed at $\Delta z = 62\,$cm, c. f. the temporal profiles shown in Fig. 7(a). The corresponding GDD for the windowed (dashed line) and windowless case (solid line) is shown in Fig. 7(b). Confirming experimental observations [Fig. 3(b)], for the windowed case, a stronger fluctuation of the GDD on the red spectral wing is observed.

6 Conclusions

Even though measurements of the pulse shape or spectral phase are virtually impossible directly at location of the output window, we managed to demonstrate that the window and its position are highly important in achieving a self-compressed pulse out of a filament compressor. Depending on the window position, the suggested self-healing mechanism can either be activated or inhibited. Windowless operation of the argon cell also clearly shows that the pulse coming directly out of the cell is already short, but its short temporal signature may then be spoilt by the sudden non-adiabatic change in dispersion and nonlinearity in a solid window. Our experiments indicate that the length of the highly dispersive and nonlinear material is of secondary importance, as even thin foils require self-healing in order to obtain a short pulse at the output of the cell. All these observation strongly support the theoretically predicted importance of the windows for shaping of a short pulse. These findings may explain that some authors experienced problems in reproducing filament self-compression in windowed cells whereas direct

self-compression in atmospheric air appeared to work right away [11, 32]. We believe that future application of this versatile compression mechanism can be greatly simplified if the position of the rear window is actively adjusted for optimum shortness of the pulse.

References

[1] C. V. Shank, R. L. Fork, R. Yen, R. H. Stolen and W. J. Tomlinson, Appl. Phys. Lett. **40**, 761 (1982).

[2] M. Nisoli, S. DeSilvestri, O. Svelto, R. Szikops, K. Ferencz, C. Spielmann, S. Sartania and F. Krausz Opt. Lett. **22**, 522 (1997).

[3] M. Nisoli, S. De Silvestri, and O. Svelto Appl. Phys. Lett. **68**, 2793 (1996).

[4] G. Steinmeyer and G. Stibenz, Appl. Phys. B **82**, 175 (2006).

[5] A. Suda and M. Hatayama, K. Nagasaka, and K. Midorikawa, Appl. Phys. Lett. **86**, 111116 (2005).

[6] C. P. Hauri, W. Kornelis, F. W. Helbing, A. Heinrich, A. Couairon, A. Mysyrowicz, J. Biegert and U. Keller, Appl. Phys. B **79**, 673, (2004).

[7] S. Adachi, N. Ishii, Y. Nomura, Y. Kobayashi, J. Itatani, T. Kanai, and S. Watanabe, Opt. Lett. **35**, 980 (2010).

[8] G. Stibenz, N. Zhavoronkov, and G. Steinmeyer, Opt. Lett. **31**, 274 (2006).

[9] S. Skupin, G. Stibenz, L. Berge, F. Lederer, T. Sokollik, M. Schnürer, N. Zhavoronkov, and G. Steinmeyer. Phys. Rev. E **74**, 056604 (2006).

[10] A. Zaïr, A. Guandalini, F. Schapper, M. Holler, J. Biegert, L. Gallmann, A. Couairon, M. Franco, A. Mysyrowicz, and U. Keller, Opt. Express **15**, 5394 (2007).

[11] O. G. Kosareva, N. A. Panov, D. S. Uryupina, M. V. Kurilova, A. V. Mazhorova, A. B. Savel'ev, R. V. Volkov, V. P. Kandidov, and S. L. Chin, Appl. Phys. B **91**, 35 (2008).

[12] S. Backus, C. G. Durfee III, M. M. Murnane, and H. C. Kapteyn, Rev. Sci. Instrum. **69**, 1207 (1997).

[13] L. Bergé, S. Skupin and G. Steinmeyer, Phys. Rev. Lett. **101**, 213901 (2008).

[14] L. Bergé, S. Skupin, and G. Steinmeyer, Phys. Rev. A **79**, 033838 (2009).

[15] C. Iaconis and I. A. Walmsley. Opt. Lett. **23**, 792 (1998).

[16] C. Iaconis and I. A. Walmsley, IEEE J. Quantum Electron. **35**, 501 (1999).

[17] L. Gallmann, D. H. Sutter, N. Matuschek, G. Steinmeyer, U. Keller, C. Iaconis, and I. A. Walmsley, Opt. Lett. **24**, 1314 (1999).

[18] G. Stibenz and G. Steinmeyer, Rev. Sci. Instrum. **77**, 073105 (2006).

[19] A. L. Gaeta, Phys. Rev. Lett. **84**, 3582 (2000).

[20] L. Bergé and S. Skupin, Phys. Rev. Lett. **100**, 113902 (2008).

[21] Using a band gap of 3.8 eV [S. A. Y. Al-Ismail and C. A. Hogarth, J. Mat. Sci. Lett. **7**, 135 (1988)] and $n = 1.5$, we estimate a nonlinear refractive index $n_2 = 2 \times 10^{-15}$ cm^2/W for polypropylene at 800 nm. This estimation is based on [M. Sheik-Bahae, D. C. Hutchings, D. J. Hagan, E. W. Van Stryland, IEEE J. Quantum Electron. **27**, 1296 (1993).]. A group velocity dispersion $\beta_2 = 300$ fs^2/mm is indicated in [T. Yovcheva, T. Babeva, K. Nikolova, and G. Mekishev, J. Opt. A**10**,055008 (2008)]. These values are at least 5 times larger than the characteristic values for silica at the same wavelength.

[22] T. Brabec and F. Krausz, Phys. Rev. Lett. **78**, 3282 (1997).

[23] A. Dalgarno and A. E. Kingston, Proc. Roy. Soc. A **259**, 424 (1960).

[24] H. J. Lehmeier, W. Leupacher, and A. Penzkofer, Opt. Commun. **56**, 67 (1985).

[25] J. -F. Daigle, O. Kosareva, N. Panov, M. Bégin, F. Lessard, C. Marceau, Y. Kamali, G. Roy, V. Kandidov, and S. Chin, Appl. Phys. B **94**, 249 (2009).

[26] C. Brée, A. Demircan, S. Skupin, L. Bergé, and G. Steinmeyer. Opt. Express **17**, 16429 (2009).

[27] C. Brée, J. Bethge, S. Skupin, L. Bergé, A. Demircan, and G. Steinmeyer, New J. Phys. **12**, 093046 (2010).

[28] P. Sprangle, J. R. Peñano, and B. Hafizi, Phys. Rev. E **66**, 046418 (2002).

[29] E. T. J. Nibbering, G. Grillon, M. A. Franco, B. S. Prade, and A. Mysyrowicz, J. Opt. Soc. Am. B **14**, 650 (1997).

[30] J. R. Peñano, P. Sprangle, B. Hafizi, W. Manheimer, and A. Zigler, Phys. Rev. E **72**, 036412 (2005).

[31] S. Linden, H. Giessen, and J. Kuhl, physica status solidi (b) **206**, 119 (1998).

[32] B. E. Schmidt, W. Unrau, A. Mirabal, S. Li, M. Krenz, L. Wöste, and T. Siebert, Opt. Express **16**, 18910 (2008).